Plane-wave final state for photoemission from nonplanar molecules at a metal-organic interface

C. Metzger,[1] M. Graus,[1] M. Grimm,[1] G. Zamborlini,[2,3] V. Feyer,[2] M. Schwendt,[4] D. Lüftner,[4] P. Puschnig,[4] A. Schöll,[1] and F. Reinert[1]

[1]*Julius-Maximilians-Universität Würzburg, Experimentelle Physik VII, 97074 Würzburg, Germany*
[2]*Forschungszentrum Jülich, Peter Grünberg Institut, 52425 Jülich, Germany*
[3]*Technische Universität Dortmund, Experimentelle Physik VI, 44227 Dortmund, Germany*
[4]*Karl-Franzens-Universität Graz, Institut für Physik, NAWI Graz, 8010 Graz, Austria*

(Received 27 August 2019; accepted 5 March 2020; published 21 April 2020)

In recent years, the method of orbital tomography has been a useful tool for the analysis of a variety of molecular systems. However, the underlying plane-wave final state has been largely expected to be applicable to planar molecules only. Here, we demonstrate on photoemission data from the molecule C_{60} adsorbed on Ag(110) that it can indeed be a valid approximation for truly three-dimensional molecules at a metal-organic interface. A comparison of the experimental data supported by density functional theory (DFT) calculations of the full interface and simulations of the photoemission process with a more exact final state enables the determination of the adsorption geometry and orientation of the C_{60} molecules in a monolayer on the Ag(110) surface. Additionally, charge transfer into the molecules is used to confirm the lifting in degeneracy of the t_{1u} molecular orbitals as predicted by DFT calculations.

DOI: 10.1103/PhysRevB.101.165421

I. INTRODUCTION

Angle-resolved photoelectron spectroscopy (ARPES) is a well-established technique for the determination of electronic bands and energy levels within a system. It is a powerful investigative tool due to the connection between the photoelectrons and the electronic structure of the sample, which enables the extraction of structural [1–3], electronic [4–6], and chemical information [7,8]. A common theoretical description of the final state is the use of a plane wave. However, this approximation has generally been expected to be suitable exclusively for planar molecules [9]. Due to a lack of data on this topic, the applicability of the plane-wave final state beyond these constraints is still an open question.

Our study presents a comprehensive scheme to examine this issue on the example of a monolayer of the nonplanar and nearly spherically symmetric fullerene C_{60} on Ag(110). We focus on the applicability of the plane-wave approximation when the molecules are interacting with the metal surface. Thicker films will be discussed in a related paper in which molecule-molecule interactions are dominant and molecular bands appear in the valence region [10]. In that case, molecule-molecule interactions are dominant and molecular bands appear in the valence region.

Fullerenes have been the target of extensive fundamental research over the past decades and abundant applications are envisioned for its various derivatives [11–13]. C_{60} is an organic electron acceptor [14] that is resistant against mechanical and environmental strains [15] and is already being used in devices [16–18]. Previous photoemission efforts shed light on photoemission intensity resonances induced by the geometric shape of C_{60} [19,20] and the electronic band dispersion in high-quality thin films [21]. The experimental data on the C_{60}/Ag(110) interface are supported by density functional theory (DFT) calculations and simulations of the photoemission matrix elements. We expect that our approach on this model system can be transferred to investigate and understand other metal-organic interfaces.

II. EXPERIMENTAL DETAILS

Experiments were conducted at the NanoESCA beamline of the Elettra synchrotron in Trieste, Italy. A single layer of commercially available C_{60} (99.9% purity, Sigma-Aldrich) was evaporated on an Ag(110) substrate that had previously been cleaned by several cycles of argon ion bombardment with subsequent thermal annealing. The molecules were deposited from a homemade thermal evaporator at a rate of 40 min per monolayer that had been determined from previous x-ray photoemission and low-energy electron diffraction (LEED) experiments. Followed by another annealing step of the sample at 300 °C for 5 min to increase the homogeneity of the film, the successful preparation of the C_{60} monolayer was verified by LEED. The evaporation and all consecutive measurements were performed with the sample at room temperature.

Figure 1(a) shows the LEED pattern of the resulting sample surface for an electron kinetic energy of 12 eV. The Ag(110) surface promotes the assembly of molecules in an ordered superstructure, which is reproduced by a $(1.67, 2/1.67, -2)$ superstructure matrix as indicated in the picture (red circles). This corresponds to a C_{60} nearest-neighbor spacing of 94% of the bulk value at room temperature [22].

Angle-resolved photoemission experiments on the sample were carried out with a photoemission electron microscope in a k-space imaging mode (k-PEEM) with an energy resolution of ∼100 meV [23]. The photoemission intensity in the valence

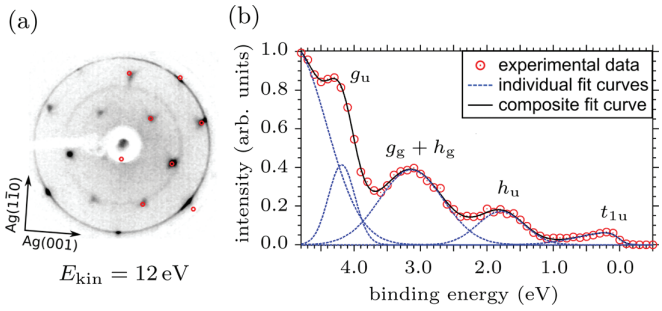

FIG. 1. (a) LEED pattern of a single monolayer of C_{60} on an Ag(110) substrate with a primary electron energy of 12 eV. Positions of constructive interference to be expected with a $(1.67, 2/1.67, -2)$ superstructure matrix are indicated by red circles. (b) Corresponding exemplary energy distribution curve (EDC) with right-circularly polarized light at a photon energy of $E_{ph} = 42$ eV (red dots). The EDC is fitted by the black line with the individual fit components represented by dashed blue lines.

region at binding energies from 5 eV below to 0.5 eV above the Fermi level was recorded under illumination with right-circularly polarized light using photon energies between 20 and 140 eV. The light polarization was chosen to suppress the higher harmonics of the undulator source.

Figure 1(b) depicts an exemplary energy distribution curve (EDC) at a photon energy of 42 eV (red dots). The intensity from the silver substrate is suppressed by the adsorption of the C_{60} monolayer. At binding energies larger than ~4 eV, however, the silver 4*d* bands dominate the photoemission spectrum. Four features within the scanned range can be attributed to C_{60}, as indicated by the symmetry labels. Note that due to the high symmetry of C_{60}, each of these molecular orbitals would be several times degenerate for the isolated molecule. While the symmetry is disturbed by the presence of the substrate and adjacent molecules, the lifted degeneracy cannot be straightforwardly resolved within the energy resolution. It therefore only increases the width of the features. As illustrated in Fig. 1(b), molecular features whose energy separation is below the resolution limit are accordingly summarized under a shared moniker indicating their combined symmetry. We have tentatively assigned the molecular emissions around 4.3, 3.2, 1.8, and 0.2 eV to the g_u, $g_g + h_g$, h_u, and t_{1u} orbitals of C_{60}. A modest amount of charge transfer from the substrate into the molecules' lowest unoccupied molecular orbital (LUMO) (t_{1u}) can be identified by the increased photoemission intensity right at and below the Fermi edge, a property frequently observed in similar systems [24,25].

III. THEORY

Ab initio simulations of the ground-state electronic structure or, ideally, of the entire photoemission process, can yield insights not immediately accessible from the experimental data alone. Consequently, DFT calculations have been performed on an isolated C_{60} molecule using Gaussian 09W [26] with a 6-31G+ basis set relying on the linear combination of atomic orbitals (LCAO) and the Becke three-parameter Lee-Yang-Parr (B3LYP) functional [27,28]. The resulting initial states were subsequently used in quantifying the matrix elements of Fermi's golden rule together with final states in the independent atomic center approximation (IAC) in a one-step model of photoemission. The computational scheme is similar to methods already described in the literature [25,29–31]. The photoemission intensity $I_n(\vec{k})$ at wave vector $\vec{k}$ of a molecular orbital n is described as the coherent superposition of all atomic contributions,

$$I_n(\vec{k}) \propto \left| \sum_a \langle \psi_{f,a} | \vec{\epsilon} \cdot \vec{r} | \psi_{i,a}(\vec{k}) \rangle \right|^2, \tag{1}$$

with the interaction operator $\vec{\epsilon} \cdot \vec{r}$ of the incoming electromagnetic field and the partial initial and final states $\psi_{i,a}$ and $\psi_{f,a}$ at atom a, respectively.

The final state is analogously the coherent superposition of partial final states $\psi_{f,a}$ at each atomic site a,

$$\psi_{f,a} = 4\pi \sum_{l=0}^{\infty} \sum_{m=-l}^{l} i^l j_l(kr) Y_{l,m}(\hat{r}) Y^*_{l,m}(\hat{k}) D_a(k) \delta^l_a(k) e^{-i\vec{k}\vec{R}_a}, \tag{2}$$

with spherical Bessel functions j_l, spherical harmonics $Y_{l,m}$, inelastic damping D_a, and phase shift δ^l_a from the potential of the emitting atom a. The interaction operator is taken from the known geometry and light polarization in the experiment. The intensity of molecular orbitals which cannot be energetically separated in the experiment are incoherently summed up after the matrix element calculation. For comparison, we have also calculated photoelectron momentum maps (PMMs) by approximating the final state by a plane wave following the approach in Ref. [4].

Additionally, we have performed calculations for monolayers of C_{60} adsorbed on the Ag(110) surface with the VASP code [32]. We have employed a repeated slab approach, where the substrate was modeled by five metallic layers, and a vacuum layer of ~15 Å between the slabs. To avoid spurious electrical fields, a dipole layer was inserted in the vacuum region [33]. Exchange-correlation effects have been approximated using the generalized gradient approximation (GGA) [34]. We used a Monkhorst-Pack $10 \times 10 \times 1$ grid of k points for calculations with one molecule per cell [35], and a $6 \times 6 \times 1$ grid for those with three molecules per cell. With the projector augmented-wave approach [36], this enabled using a kinetic energy cutoff of about 500 eV. The supercell geometry has been constructed according to the experimental LEED structure shown in Fig. 1(a). During the geometry optimization, the atomic positions of the molecular layer and the first two metallic layers were allowed to relax. In order to account for van der Waals (vdW) interactions, we employed the vdW-surf method according to Tkatchenko and Scheffler [37] during the geometry optimization.

IV. RESULTS AND DISCUSSION

Ahead of the data evaluation, the acquired PMMs were corrected for experimental artifacts. Afterwards the photoemission intensities of each recorded feature were extracted with a fitting procedure (see Supplemental Material for details [38]). Figure 1(b) displays an exemplary fit of an EDC for a single (k_x, k_y)-tuple at a photon energy of 42 eV. The entirely fitted PMM of the h_u orbital is displayed in Fig. 2(a) for

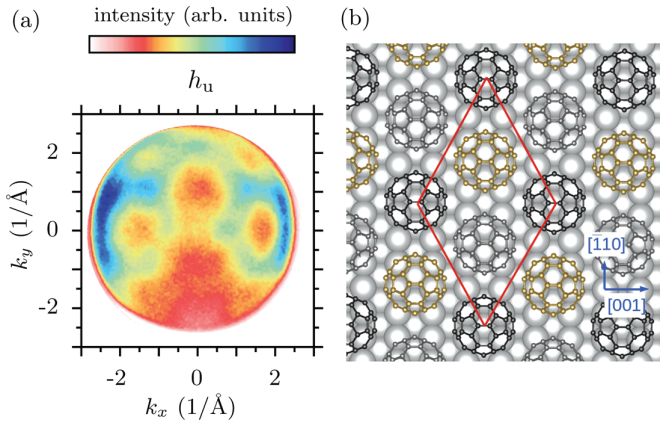

FIG. 2. (a) Fitted PMM intensity for emissions from the h_u orbital excited with $E_{ph} = 42$ eV. (b) Adsorption geometry of C_{60} on Ag(110), showing the three inequivalent C_{60} molecules per unit cell in different colors. The unit cell is indicated by red lines.

light incidence toward positive k_y values. The sudden drop in intensity at high $k_\parallel$ is not caused by the finite photoemission horizon, but by the limited extent of the multichannel plate detector.

As apparent in the fitted PMM (and likewise in the raw data), the intrinsic patterns are essentially twofold symmetric. In contrast to the bulk structure [39], this suggests that there is only one unique azimuthal orientation of C_{60} present on the Ag(110) surface at room temperature. Unlike planar molecules [40], the three-dimensional geometry of C_{60} results in a considerable photoemission intensity redistribution for varied photon energies.

We have relaxed the structure of the C_{60}/Ag(110) interface in the $c(4 \times 4)$ cell starting from five different molecular orientations, and four different adsorption sites, and computed the resulting adsorption energies according to

$$E_{\text{adsorption}} = \frac{E_{\text{system}} - E_{\text{sub}} - nE_{\text{mol}}}{n}, \tag{3}$$

where E_{system}, E_{sub}, and E_{mol} are the ground-state energies of the whole system, the silver substrate, and the molecule, respectively, while n denotes the number of molecules per unit cell. The results are listed in Table I. The orientation labels specify what part of the molecule lies parallel to the substrate. In the case of 6-6 and 5-6 the bridges between two hexagon faces (6-6) or a hexagon and a pentagon face (5-6) lie parallel to the [001] direction of the substrate. The 6-6 (90°) configuration is rotated by 90° with respect to the 6-6 configuration. Similarly, in the hexagon (pentagon) orientation, a hexagon (pentagon) face of C_{60} lies parallel to the substrate. As can be seen, the edge 6-6 orientation at the hollow site (H) has the most favorable adsorption energy, followed by the 5-6 (H), 6-6 rotated (H), and hexagon (H) configurations. Note that all other configurations are even less favorable in adsorption energy.

TABLE I. Calculated adsorption energies of C_{60} in a $c(4 \times 4)$ surface unit cell of Ag(110) for five initial C_{60} orientations and four adsorption sites: H = hollow, T = top, SB = short bridge, LB = long bridge.

	6-6	6-6 (90°)	Pentagon	Hexagon	5-6
H	−2.06	−1.90	−1.72	−1.88	−1.93
T	−1.52	−1.34	−1.13	−1.16	−1.40
SB	−1.21	−1.43	−1.45	−1.58	−1.50
LB	−1.83	−1.39	−1.72	−1.72	−1.81

While on the basis of Table I alone it cannot be safely concluded that C_{60} is exclusively in the 6-6 edge configuration, the twofold symmetry of the PMMs rules out the hexagon and 6-6 rotated configuration. Furthermore, simulated PMMs of the 5-6 configuration (not shown) are also not in agreement with the experimental PMMs, leaving just the 6-6 configuration. Based on the results of Table I, we have calculated the C_{60}/Ag(110) interface for the experimentally determined $(1.67, 2/1.67, -2)$ superstructure. This cell contains three inequivalent C_{60} molecules per surface unit cell, all of them with 6-6 orientation [see Fig. 2(b)]. The geometry relaxation results in an adsorption energy of −2.71 eV per molecule. It should be noted that although only one C_{60} molecule is positioned at the most favorable hollow site while the other two are close to the long bridge sites, the average adsorption energy per molecule indicates a more stable structure compared to the larger $c(4 \times 4)$ cell. This is because of increased intermolecular interactions for the more densely packed molecules in this cell and by the fact that the 6-6 (LB) configuration is only slightly less favorable than the 6-6 (H) one.

Starting from the relaxed adsorption geometry, photoemission matrix elements have been computed for several molecular configurations on the substrate. In agreement with the geometry relaxation, a decent match between experiment and simulation is only achieved for the 6-6 orientation. The simulated PMMs for this geometry are compared to the respective measurement in Fig. 3. The left column shows the $g_g + h_g$ orbital of the experiment [Fig. 3(a)], the calculation with a plane-wave final state [Fig. 3(c)], and with a IAC-based final state [Fig. 3(e)]. An analogous comparison is displayed for the experimental [Fig. 3(b)], plane-wave-based [Fig. 3(d)], and IAC-based [Fig. 3(e)] PMMs of the h_u orbital. Both types of calculations reproduce the goggle-shaped features of the experiment fairly well, with only small differences in the relative intensities between both simulation methods. In general, the IAC-based simulations manage to reproduce the relative intensities at different $k_\parallel$ slightly better. This largely decent agreement between simulation and experiment is maintained at other photon energies (see Supplemental Material [38] for a comparison at $E_{ph} = 32$, 50, and 60 eV).

Since the IAC-based simulations are computed with an isolated molecule, this permits an assertion about the hybridization and the molecular deformation upon adsorption. Even though there is some charge transfer from the substrate into the organic monolayer, the hybridization with neighboring C_{60} molecules and the Ag(110) substrate is evidently not strong enough to substantially alter the character of these valence orbitals. Neither is there any atomic displacement on the silver surface large enough to affect the PMM. This conclusion is consistent with the well-established rigidity of C_{60} [41].

DFT calculations of the relaxed molecule on the silver surface performed with the VASP code predict the charge transfer into the molecules that is confirmed by the experiment

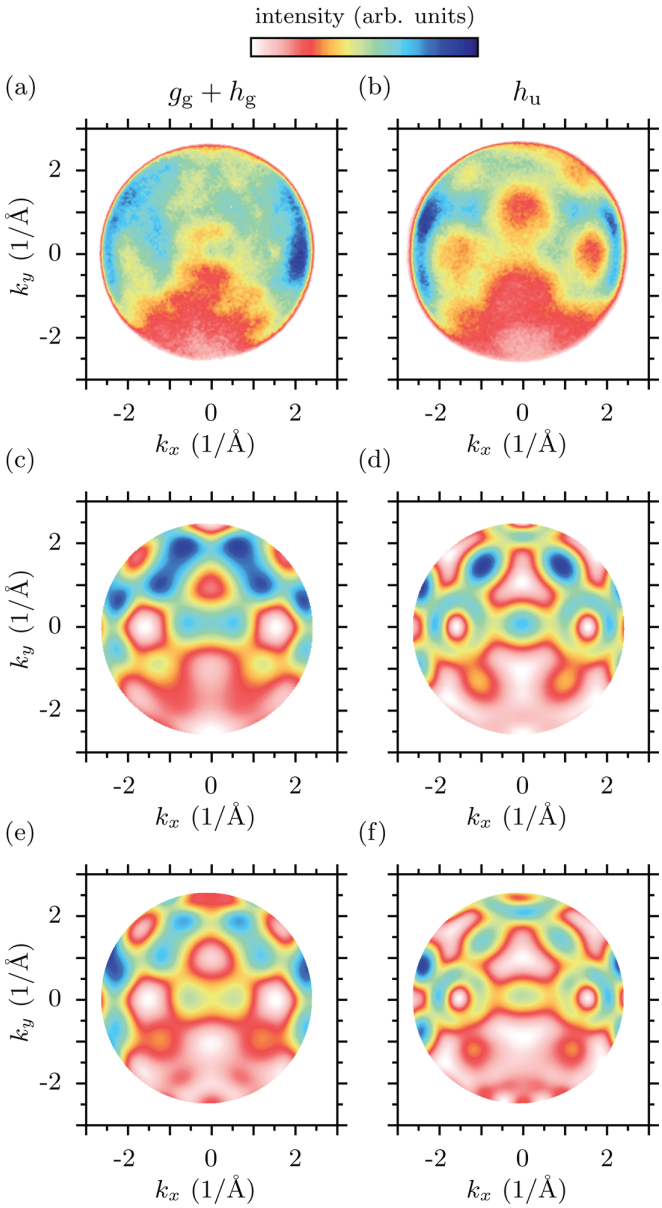

FIG. 3. Experimental PMM (top) in comparison to simulations with final states based on the plane-wave approximation (middle) and the IAC approximation (bottom) at 40 eV photon energy. The left column shows the $g_g + h_g$ orbitals, and the right column the h_u orbitals. Both types of simulations fit well to the experimental data with only minor deviations in intensity.

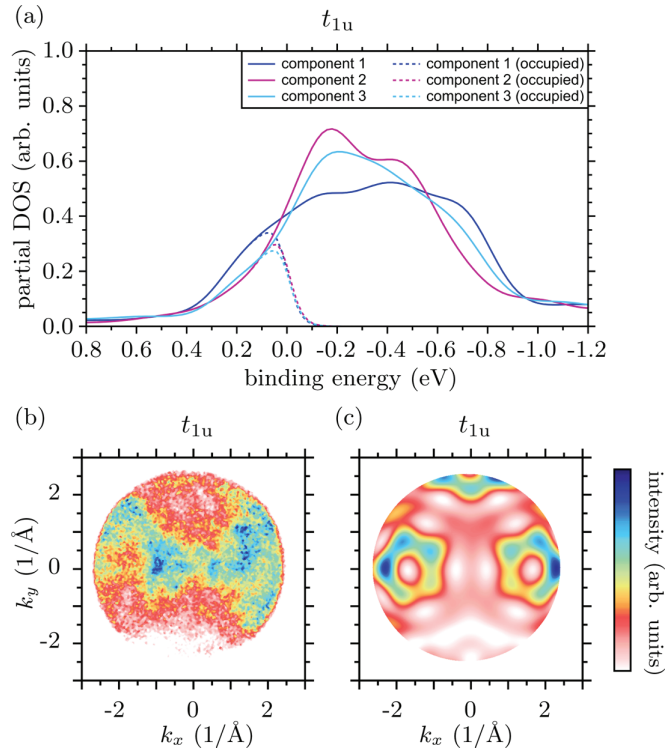

FIG. 4. (a) Calculated projected density of states (DOS) of the C_{60}/Ag(110) system, demonstrating the degeneracy lifting of the t_{1u} orbitals upon adsorption. Comparison of the PMM of the measured t_{1u} orbital (b) to an IAC-based simulation (c) for a photon energy of 40 eV.

[see Fig. 1(b)]. Furthermore, while the symmetry breaking upon adsorption does not influence the $g_g + h_g$ and h_u photoemission, it is not entirely without significance: The calculations reveal a small energetic redistribution of the formerly threefold degenerate t_{1u} which lifts the degeneracy of the three orbitals, shown in Fig. 4(a). Integrating the fractional occupation of the three components results in a relative occupation of 39%, 31%, and 30% with respect to each other.

With this knowledge, further photoemission calculations of the t_{1u} can be conducted and correlated to the experiment. Figure 4(b) shows the measured photoemission intensity at 40 eV compared to the fitted [Fig. 4(c)] with simulations of the t_{1u} with the IAC approximation. The fractional occupation numbers have been taken into account by multiplying the PMMs of the three components by their respective factor. Note that the relatively small charge transfer into the t_{1u} [see Fig. 1(b)] results in a low signal-to-noise ratio, making the quantitative analysis more demanding.

The PMM shows a goggle-shaped feature with increased intensity towards higher $|k_x|$ and from low to high k_y values. The drop in intensity around $k_x = \pm 1.7$ Å^{-1} and $k_y = 0$ is also visible in both PMMs. Even though the match between experiment and theory is not as good as for the $g_g + h_g$ and h_u under these conditions, the general shape and intensity distribution fits moderately well, corroborating the DFT result from the relaxed molecule.

In conclusion, we have demonstrated that despite previous reservations [9], the plane-wave final state can be successfully applied in photoemission calculations for nonplanar molecules at a metal-organic interface. Our comparison of simulations with the plane-wave final state with an IAC final state and the experiment shows a decent agreement. We have characterized the C_{60}/Ag(110) interface through photoemission in a combined approach of state-of-the-art measurements, intricate data evaluation, and theoretical simulations. The adsorption site, deformation, and orientation of C_{60} were computed and the latter confirmed experimentally. The weak hybridization between substrate and molecules has been revealed and DFT calculations of the redistributed density of states of the formerly degenerate t_{1u} have been verified in the

experiment. The molecules are only negligibly distorted upon adsorption and do not hybridize significantly with each other.

ACKNOWLEDGMENTS

We thank K. Waltar, A. Schuler, L. Castiglioni (Universität Zürich), P. Krüger (Chiba University), and K. Baumgärtner (Universität Würzburg) for helpful discussions. C.M., M.G., M.G., A.S., and F.R. acknowledge support by the Deutsche Forschungsgemeinschaft through Projects No. RE1469/12-2 and No. SCHO1260/4-2 as well as by the Japan Society for the Promotion of Science during the Summer Program 2018. M.S. and P.P. acknowledge support from the Austrian Science Fund (FWF) through Project No. I3731. The computations have been partially performed on the facilities of the KFU Graz and of the Vienna Scientific Cluster.

[1] M. Wießner, D. Hauschild, A. Schöll, F. Reinert, V. Feyer, K. Winkler, and B. Krömker, Phys. Rev. B **86**, 045417 (2012).
[2] B. Stadtmüller, M. Willenbockel, E. Reinisch, T. Ules, F. Bocquet, S. Soubatch, P. Puschnig, G. Koller, M. Ramsey, F. Tautz *et al.*, Europhys. Lett. **100**, 26008 (2012).
[3] V. Feyer, M. Graus, P. Nigge, M. Wießner, R. Acres, C. Wiemann, C. Schneider, A. Schöll, and F. Reinert, Surf. Sci. **621**, 64 (2014).
[4] P. Puschnig, S. Berkebile, A. J. Fleming, G. Koller, K. Emtsev, T. Seyller, J. D. Riley, C. Ambrosch-Draxl, F. P. Netzer, and M. G. Ramsey, Science **326**, 702 (2009).
[5] M. Dauth, M. Wiessner, V. Feyer, A. Schöll, P. Puschnig, F. Reinert, and S. Kümmel, New J. Phys. **16**, 103005 (2014).
[6] S. Jakobs, A. Narayan, B. Stadtmuüller, A. Droghetti, I. Rungger, Y. S. Hor, S. Klyatskaya, D. Jungkenn, J. Stoückl, M. Laux *et al.*, Nano Lett. **15**, 6022 (2015).
[7] J. Ziroff, F. Forster, A. Schöll, P. Puschnig, and F. Reinert, Phys. Rev. Lett. **104**, 233004 (2010).
[8] M. Wießner, J. Ziroff, F. Forster, M. Arita, K. Shimada, P. Puschnig, A. Schöll, and F. Reinert, Nat. Commun. **4**, 1514 (2013).
[9] A. M. Bradshaw and D. P. Woodruff, New J. Phys. **17**, 013033 (2015).
[10] N. Haag, D. Lüftner, F. Haag, J. Seidel, L. L. Kelly, G. Zamborlini, M. Jugovac, V. Feyer, M. Aeschlimann, P. Puschnig, M. Cinchetti, and B. Stadtmüller, Phys. Rev. B **101**, 165422 (2020).
[11] H. W. Kroto, J. R. Heath, S. C. O'Brien, R. F. Curl, and R. E. Smalley, Nature (London) **318**, 162 (1985).
[12] Y. Zhao, Y. Gai, S. Jin, X. Tong, J. Zhang, and E. Yifeng, Sci. Adv. Mater. **11**, 502 (2019).
[13] Y. Ishikawa, T. Hasegawa, and C. Joachim, Jpn. J. Appl. Phys. **58**, SDDF02 (2019).
[14] J. L. Segura, N. Martín, and D. M. Guldi, Chem. Soc. Rev. **34**, 31 (2005).
[15] S. Günes, H. Neugebauer, and N. S. Sariciftci, Chem. Rev. **107**, 1324 (2007).
[16] R. Haddon, A. Perel, R. Morris, T. T. Palstra, A. Hebard, and R. Fleming, Appl. Phys. Lett. **67**, 121 (1995).
[17] K. Wojciechowski, T. Leijtens, S. Siprova, C. Schlueter, M. T. Hoürantner, J. T.-W. Wang, C.-Z. Li, A. K.-Y. Jen, T.-L. Lee, and H. J. Snaith, J. Phys. Chem. Lett. **6**, 2399 (2015).
[18] W. Lv, Y. Liang, Q. Dai, J. Zhou, Z. Zhou, F. Lu, S. Xu, H. Zhang, L. Sun, and Y. Peng, Synth. Met. **250**, 131 (2019).
[19] Y. B. Xu, M. Q. Tan, and U. Becker, Phys. Rev. Lett. **76**, 3538 (1996).
[20] S. Hasegawa, T. Miyamae, K. Yakushi, H. Inokuchi, K. Seki, and N. Ueno, Phys. Rev. B **58**, 4927 (1998).
[21] D. W. Latzke, C. Ojeda-Aristizabal, S. M. Griffin, J. D. Denlinger, J. B. Neaton, A. Zettl, and A. Lanzara, Phys. Rev. B **99**, 045425 (2019).
[22] P. A. Heiney, J. E. Fischer, A. R. McGhie, W. J. Romanow, A. M. Denenstein, J. P. McCauley Jr, A. B. Smith, and D. E. Cox, Phys. Rev. Lett. **66**, 2911 (1991).
[23] C. M. Schneider, C. Wiemann, M. Patt, V. Feyer, L. Plucinski, I. Krug, M. Escher, N. Weber, M. Merkel, O. Renault *et al.*, J. Electron Spectrosc. Relat. Phenom. **185**, 330 (2012).
[24] A. Mugarza, R. Robles, C. Krull, R. Korytár, N. Lorente, and P. Gambardella, Phys. Rev. B **85**, 155437 (2012).
[25] M. Grimm, C. Metzger, M. Graus, M. Jugovac, G. Zamborlini, V. Feyer, A. Schöll, and F. Reinert, Phys. Rev. B **98**, 195412 (2018).
[26] M. Frisch, G. Trucks, H. Schlegel, G. Scuseria, M. Robb, J. Cheeseman, G. Scalmani, V. Barone, B. Mennucci, G. Petersson *et al.*, *Gaussian 09, Revision A.02* (Gaussian Inc., Wallingford, CT, 2009).
[27] A. D. Becke, J. Chem. Phys. **98**, 5648 (1993).
[28] C. Lee, W. Yang, and R. G. Parr, Phys. Rev. B **37**, 785 (1988).
[29] A. Liebsch, Phys. Rev. B **13**, 544 (1976).
[30] T. Fujikawa and H. Arai, J. Electron Spectrosc. Relat. Phenom. **123**, 19 (2002).
[31] S. Hasegawa, S. Tanaka, Y. Yamashita, H. Inokuchi, H. Fujimoto, K. Kamiya, K. Seki, and N. Ueno, Phys. Rev. B **48**, 2596 (1993).
[32] G. Kresse and J. Furthmüller, Comput. Mater. Sci. **6**, 15 (1996).
[33] J. Neugebauer and M. Scheffler, Phys. Rev. B **46**, 16067 (1992).
[34] J. P. Perdew, K. Burke, and M. Ernzerhof, Phys. Rev. Lett. **77**, 3865 (1996).
[35] M. Methfessel and A. T. Paxton, Phys. Rev. B **40**, 3616 (1989).
[36] G. Kresse and D. Joubert, Phys. Rev. B **59**, 1758 (1999).
[37] A. Tkatchenko and M. Scheffler, Phys. Rev. Lett. **102**, 073005 (2009).
[38] See Supplemental Material at http://link.aps.org/supplemental/10.1103/PhysRevB.101.165421 for details on the experimental data treatment and fitting procedures, and a figure comparing the measurements to the calculations at photon energies $E_{\mathrm{ph}} =$ 32, 50, and 60 eV.
[39] C. Yannoni, R. Johnson, G. Meijer, D. Bethune, and J. Slem, J. Phys. Chem. **95**, 9 (1991).
[40] S. Weiß, D. Lüftner, T. Ules, E. M. Reinisch, H. Kaser, A. Gottwald, M. Richter, S. Soubatch, G. Koller, M. G. Ramsey, F. S. Tautz, and P. Puschnig, Nat. Commun. **6**, 8287 (2015).
[41] G. Luengo, S. E. Campbell, V. I. Srdanov, F. Wudl, and J. N. Israelachvili, Chem. Mater. **9**, 1166 (1997).